ACS Photonics

pubs.acs.org/journal/apchd5

Article

Light-Induced Trap Reduction in Organic Shortwave Infrared Photodetectors

Ning Li,* Naresh Eedugurala, Jason D. Azoulay, and Tse Nga Ng*

Cite This: https://doi.org/10.1021/acsphotonics.2c01504

Read Online

ACCESS | Metrics & More | Article Recommendations | Supporting Information

ABSTRACT: The distribution of trap states in an organic electronic device plays a critical role in their optoelectronic performance. These traps not only hinder the transport of photogenerated carriers but also cause severe recombination, thus deteriorating the overall photoresponse in the detector. Understanding and eliminating the traps in an organic photodetector is essential to promote and stabilize the response performances. This work examines the effects of trap distribution on the photoresponse performance in a shortwave infrared light detector, by interpreting charge transport dynamics and impedance characteristics. It is found that traps remaining in the device hinder the charge transport and collection in the detector because the traps can serve as recombination centers that deteriorate the photoresponse. The analysis of charge collection efficiency from current−voltage characteristics also validates this hypothesis. A dramatic trap reduction is realized by a proper exposure of the device to high-energy photons, which largely improves and stabilizes the photoresponse of the organic photodiode. It is also observed that the light-induced trap reduction is dependent on the wavelength and light intensity. The findings in this work reveal the fundamental mechanisms in the narrow-bandgap infrared sensing systems, paving the way for practical and stable infrared sensing application settings.

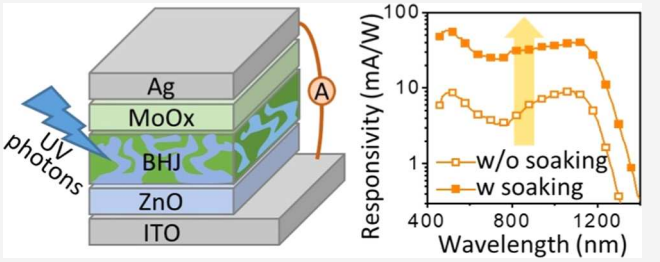

KEYWORDS: *shortwave infrared light detection, density of states, trap distribution, trap reduction, light soaking effect, impedance spectroscopy*

INTRODUCTION

The sensing and imaging of infrared photons are essential technologies in a variety of applications including industrial, military, and civilian settings, covering areas such as safety monitoring, medical diagnostics, optical communication, and so on.[1−7] Compared to traditional epitaxial inorganic infrared technology, solution-processable organic infrared semiconductor-based sensing systems are under rapid development, rendering them appealing for next-generation flexible and large-area optoelectronics due to their versatile chemical, optical, and mechanical characteristics.[5,7−9] Organic semiconducting system aiming for infrared light detection is one of the most promising research topics in organic electronics.[10−12] High photoresponse and tunable response spectrum have been realized by advancing the material synthesis and manipulating the device engineering.[13−18]

However, besides the much-improved performances in photoresponse, the stability and durability of the organic infrared devices remain an obstacle for practical applications.[5,8] It is noted that the stability of organic devices usually stems from simultaneously extrinsic and intrinsic instabilities.[19−22] The extrinsic instability originates from humidity, and oxygen exposure, which leads to the deterioration of the device performance.[23−26] On the other hand, the intrinsic instability of organic devices is usually correlated to material degradation as a function of time or light stress, e.g., delamination, material dimerization, and mutual interaction.[21] It should be noted that organic devices can be ultrastable even under high-intensity stress.[27]

However, the intrinsic disorder characteristics of organic semiconducting materials inherently exhibit traps that are detrimental to the photoresponse. Meanwhile, the vulnerability of the organic layers to oxygen or humidity would deteriorate the overall photoresponse and device stability.[28−30] It is found that the instability of the organic devices typically stems from the traps that are associated with inherent material disorders or defects created after exposing the material to ambient air, which lower the charge mobility,[24] disturb field distribution inside the device,[31] and serve as recombination centers for photogenerated charges,[32−34] as well as the origin of dark currents in the device.[35,36] It is thus concluded that materials

Received: September 27, 2022

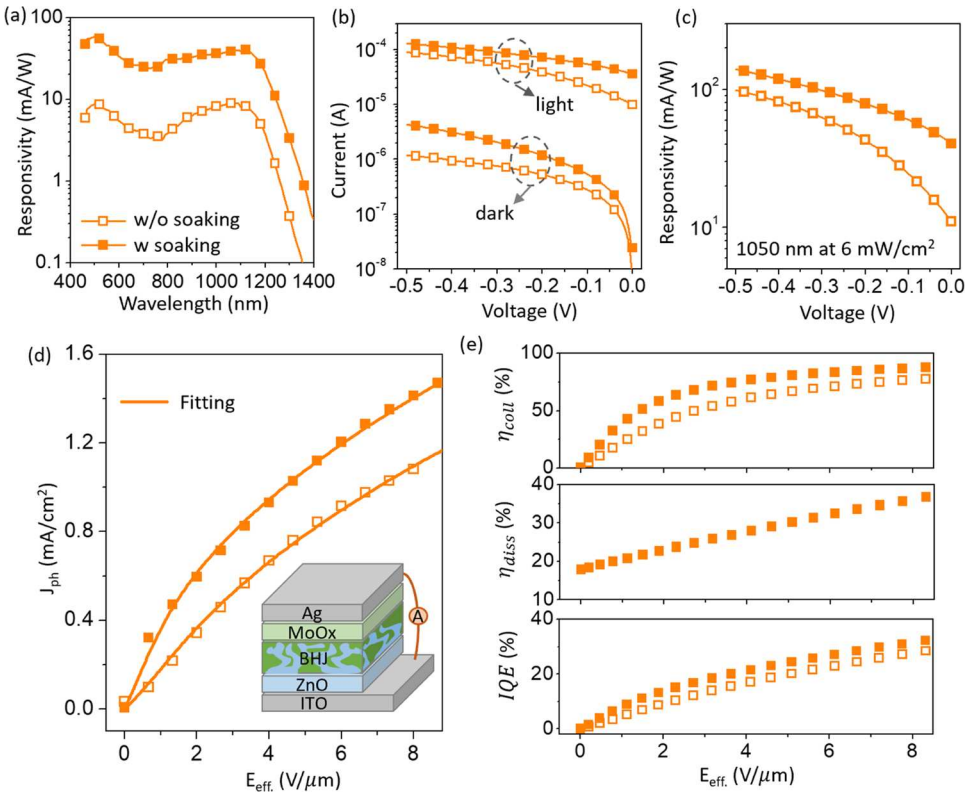

Figure 1. Photoresponse characteristics of the detector with and without light soaking. The light soaking is performed under white light from a tungsten lamp at an intensity of ~20 mW/cm^2 for 3 min. (a) Spectral photoresponse measured at 0 V. (b) Bias-dependent current−voltage relationship and (c) the corresponding responsivity measured under 1050 nm (~6 mW/cm^2). The photocurrent extracted from (b) is fitted in (d) using a theoretical model, and the corresponding efficiencies are extrapolated in (e), including the collection efficiency, dissociation efficiency, and internal quantum efficiency. The inset in (d) is a schematic illustration of the detector structure.

that are prone to degradation via trap generation under environmental stresses, such as ultraviolet, oxygen, and humidity, are less stable in optoelectronic devices. The nature of these intrinsic or extrinsic traps, and their physical and chemical properties, including the energetic distribution, density, and dependency on materials, are essential problems in organic electronics.

Substantial efforts have been made to mitigate the impacts of traps on the performance of organic devices.[37,38] It is observed that proper exposure of the organic devices to light (light soaking) would give rise to better performances.[39−41] Ultraviolet light-induced trap filling[41] and interface dipole reinstation[42] are proposed as reasons responsible for the improved performance after the light soaking process. However, a precise evaluation method of the traps regarding such a light-induced effect is still missing. An in-depth understanding of how the light soaking process is effective in manipulating the carrier dynamics is in urgent demand.

In this work here, we pay attention to the distribution of the trap states in a narrow-bandgap infrared detector and study the role of the traps in affecting the charge transport and collection. A specific perspective is provided to explain how light soaking is advantageous to improving the device performance by correlating the density of states (DOS), impedance spectroscopy results, and photoresponse efficiencies. The phenomenon of light-induced trap reduction is explained in detail by analyzing the current−voltage characteristics, equivalent circuit fitting, and capacitance−frequency results. The DOS distribution reveals deep trap reduction during the light soaking process, leading to much improved internal conductivity, validated by the impedance spectroscopy analysis. The dependency on the wavelength, soaking time, and aging time of the soaking effect is also investigated. The findings presented here are critical in understanding the device physics and optimizing the performance of the organic infrared detectors.

RESULTS AND DISCUSSION

In this work, a narrow-bandgap organic photodiode, with a multilayered configuration shown in Figure 1, is studied for shortwave infrared light sensing. The bulk heterojunction (BHJ) active layer is a blend of one narrow-bandgap semiconducting polymer (CDT-TQ, p-type) and one n-type acceptor material ($PC_{71}BM$, or ITIC-M, or ITIC-F) (see Table S1 for more details). The two semiconducting materials in the BHJ blend form type-II heterojunction as depicted in the energy diagram (Figure S1), featuring percolating networks in morphology (Figure 1d) for efficient photogenerated exciton dissociation and charge separation. The ZnO and MoO_x layers serve as electron and hole collection layers; the Ag and ITO layers are anode and cathode, respectively.

In the characterization experiments, it is observed that the device performance is very sensitive to light irradiance. By exposing the CDT-TQ:$PC_{71}BM$ device to the white light from the tungsten lamp (hereafter we use "light soaking" for this process) for 3 min, the photoresponse can be promoted dramatically, as seen in the spectral photoresponse presented in Figure 1a. For example, the photoresponse at 1000 nm is improved by more than 4-fold. The light-soaking-induced

https://doi.org/10.1021/acsphotonics.2c01504
ACS Photonics XXXX, XXX, XXX−XXX

improvement in photoresponse is broadband without any wavelength selectivity. This phenomenon is also evident in nonfullerene acceptor-based devices (Figure S2a), but the light-induced photoresponse improvement is less obvious compared to that in fullerene-based devices. It should be noted that light soaking for >3 min is enough to achieve a much improved and stable photoresponse in the detectors.

To understand the physical mechanisms determining the light-soaking-induced response improvement, a series of tests were conducted to illustrate how the optical and electrical characteristics of the device are correlated to its photoresponse. The improved photoresponse after light soaking can be from the increase in exciton dissociation efficiency (η_{diss}) and/or charge collection efficiency (η_{coll}) since the photoresponse is determined and proportional to light absorption efficiency (η_{abs}), exciton dissociation efficiency, and charge collection efficiency and given the fact that absorption is independent of light soaking process in our case. The exciton dissociation and charge collection efficiency can be extrapolated by analyzing the photocurrent (J_{ph}) vs the effective electric field (E_{eff}) relationship.[18]

The current−voltage characteristics for the CDT-TQ:$PC_{71}BM$ BHJ-based device before and after light soaking are presented in Figure 1b. The current from the detector under light (1050 nm) is higher after light soaking, resulting in higher responsivity, as shown in Figure 1c. The much-improved responsivity at 0 V here is in good accordance with the spectral responsivity (measured at 0 V), as shown in Figure 1a. It is interesting that there is an evident increase in the dark current in the detector as well, which most probably indicates a much-improved conductance of the device after light soaking. As a comparison, the light-soaking-induced variation of current−voltage characteristics in non-fullerene-based detectors is less significant as shown in Figure S2b,c.

It should be noted that a higher dark current is detrimental to the specific detectivity of the detector due to the increased shot noise. The shot noise from dark current is dominant at reverse bias, and it can be roughly estimated by $S_{shot} = \sqrt{2qI_{dark}}$. Note that this direct calculation would underestimate the total noise. Here, we estimate the specific detectivity of the detector using this simple assumption that shot noise dominates at 0.1 V. The corresponding specific detectivity for the CDT-TQ:$PC_{71}BM$ detector at 0.1 V is 2.5×10^{10} Jones before light soaking and 4.4×10^{10} Jones after light soaking. The increase in photoresponse after light soaking surpasses the increase in noise in our case.

In Figure 1d, the experimental data points are fitted to a model to extract the efficiencies.[18] The product of η_{diss} and η_{coll} is the internal quantum efficiency (IQE). The details of the model are explained in the Experimental Section, and the fitting parameters are presented in Table 1. From the results in Figure 1e, there is a clear improvement in charge collection efficiency (from 66 to 80% at 5 V/μm), which is the main reason for a higher photoresponse in the device with light soaking. The exciton dissociation efficiency in the device with light soaking is slightly higher than that in the pristine device, e.g., from 30 to 30.2% at 5 V/μm, but not as obvious as the difference in collection efficiency.

Table 1. Parameters Used in the Photocurrent Fitting for the CDT-TQ:$PC_{71}BM$ Device

fitting parameters	w/o soaking	with soaking
J_{sat} (mA/cm^2)	3.95	4.45
$\mu\tau$ ($\times 10^{-14}$ m^2/V)	1.7	3.3
k_R ($\times 10^7$ s^{-1})	0.75	0.74

We hypothesize that the improved charge collection efficiency most probably arises from the reduction of traps after the light soaking process. To validate this hypothesis, we first look at the DOS distribution within the bandgap of the semiconducting system in the organic detector. The sub-bandgap trap states can be extracted from the capacitance vs frequency relationship measured for the device.[17,34,36] The charges at different energy levels within the bandgap can respond to certain frequency ranges modulated by the external alternating field.[34] Both the density and depth of the traps can be determined in this technique. The details for the calculation are available in the Experimental Section. From the capacitance−frequency data measured for the CDT-TQ:$PC_{71}BM$ detector, as shown in Figure 2a, the DOS vs energy is extrapolated and presented in Figure 2b. It is worth noting that the slope of the capacitance−frequency curve is proportional to the DOS density. The sharp capacitance change in the low-frequency region in the device without light soaking (Figure 2a) gives rise to a higher distribution of states in deep states. As a result, there is a negligible difference in the exponential part of the DOS for the device with and without light soaking, but a dramatic difference is observed in the Gaussian part of the DOS distribution. The exponential component represents the bandtail states,[34] while the Gaussian component is usually responsible for the subgap states.[17] The results indicate a predominant reduction in subgap states in the semiconducting system. In general, the bandtail states arise from the material disorder while the deeper traps within the bandgap are associated with point detects, impurities, and extended defects.[34,43] It is thus anticipated that the light soaking effect in this work has nothing to do with the bandtail states but rather heals the traps that locate at the deep energetic sites,[41] probably correlated to the structural defects. The same phenomenon is also observed in ITIC-M and ITIC-F-based devices (Figure S3). The ITIC-M system exhibits less light soaking dependency, which is due to the much lower subgap DOS, similar to our previous reports.[13]

From the DOS analysis, one can conclude that light soaking suppresses the subgap trap states in the active layer. The reduction of subgap traps is essential to improve the response efficiency by reducing the charge recombination.

Besides the study of the distribution of traps as energy levels in the active layer, the internal resistance and quality of the interface can be analyzed by impedance spectroscopy.[44] The traps in a multilayered device can act as recombination centers or obstacles for charge collection. To understand the charge transport model of the detector, the Nyquist plot of the detector is fitted by equivalent circuits. The equivalent circuit is simplified to a series resistor combined with resistor−capacitor pairs[44,45] to account for different layers and interfaces in the device. The Nyquist plots (1 Hz to 1 MHz) of the CDT-TQ:$PC_{71}BM$ device before and after light soaking are presented in Figure 2c,d. There is a dramatic reduction in impedance after light soaking, which is a sign of conductance improvement,[40] and the shape of the Nyquist plot is transferred from a double-arc to a semicircle.[45,46] The fitting is first performed using standard capacitor and resistor combinations as shown in the inset of Figure S4, and the fitting results are also shown. The corresponding fitting

https://doi.org/10.1021/acsphotonics.2c01504
ACS Photonics XXXX, XXX, XXX−XXX

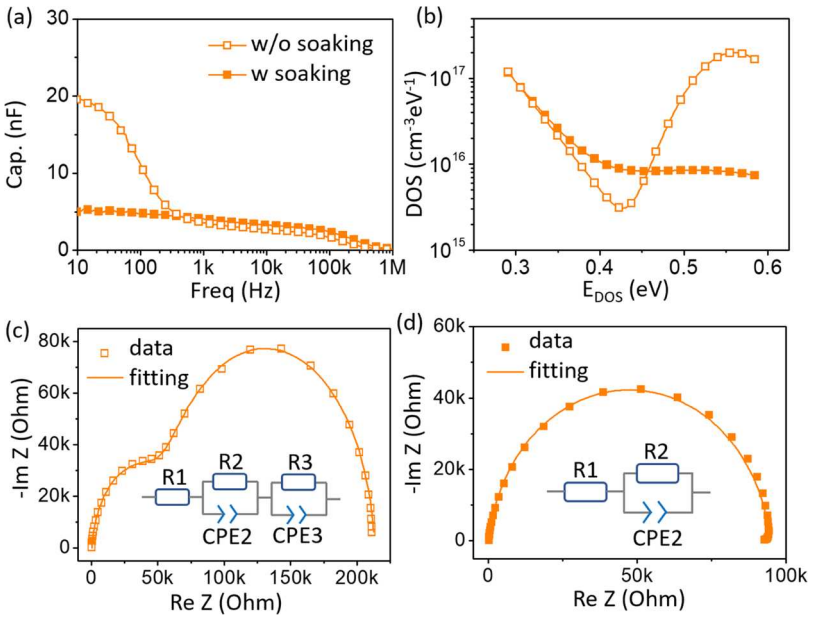

Figure 2. Subgap state distribution and impedance spectroscopy analysis for the CDT-TQ:$PC_{71}BM$ bulk heterojunction-based detector with and without light soaking process. (a) Capacitance−frequency characteristics and (b) subgap density of states extrapolated from (a). (c, d) Nyquist plot of the impedance for the detector, and their corresponding equivalent circuit fitting results. The insets in (c, d) illustrate the equivalent circuits.

Table 2. Fitting Parameters for the CDT-TQ:$PC_{71}BM$ Detector Using CPE Component

fitting parameters	w/o soaking	with soaking
R_1 (Ω)	374	212
R_2 (Ω)	5.5×10^4	9.4×10^4
CPE2	$Q_2 = 7.3 \times 10^{-9}$ ($Fs^{-0.08}$); $n_2 = 0.92$	$Q_2 = 7.4 \times 10^{-9}$ ($Fs^{-0.07}$); $n_2 = 0.93$
R_3 (Ω)	1.6×10^5	na
CPE3	$Q_3 = 4.1 \times 10^{-8}$ ($Fs^{-0.03}$); $n_3 = 0.97$	na

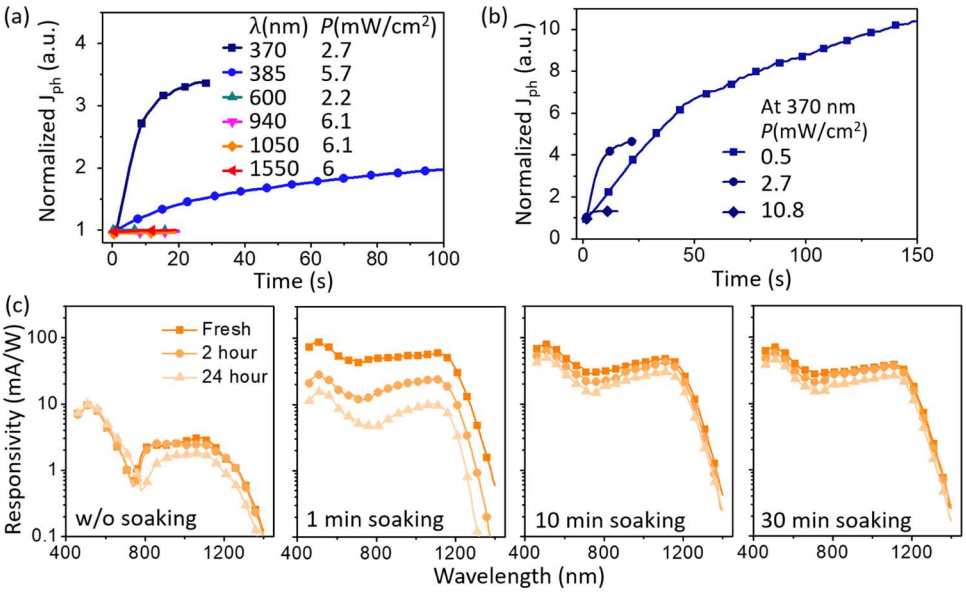

Figure 3. Wavelength, light intensity, and soaking time dependency of the light soaking effect in the CDT-TQ:$PC_{71}BM$ detector. (a) Normalized photocurrent versus time in the detector under light illumination at different wavelengths. (b) Normalized photocurrent in the detector as a function of time and light intensity at 370 nm. In (a, b), the photocurrent is normalized to the instant photonic response before the light soaking induced by the continuous light illumination of each wavelength. (c) Responsivity of the detector as a function of soaking time and aging time.

parameters are provided in Table S2. From these results, the fitting is a bit off the measured data in both cases, which is most probably due to the nonperfect interfaces in the device.[46]

To account for this nonperfection, a constant phase element (CPE)[44,46] is used in the fitting to compensate for the phase uncertainty, which is caused by material inhomogeneity.[44] The

https://doi.org/10.1021/acsphotonics.2c01504
ACS Photonics XXXX, XXX, XXX−XXX

definition of the CPE is explained in the Experimental Section. The corresponding fitting results and the equivalent circuits are presented in Figure 2c,d. The upgraded fitting model by replacing the standard capacitor with a CPE is more precise to account for the measured data, which is readily practical to unravel the underlying physical mechanism of the device.

The fitting details are summarized in Table 2. There is a clear reduction in the internal resistance (mainly shunt resistance), from $R_2 = 5.5 \times 10^4$, $R_3 = 1.6 \times 10^5$ to $R_2 = 9.4 \times 10^4$ Ω after the light soaking process. This is in good accordance with the dark current−voltage characteristics. The transition of the Nyquist plot from a double-arc feature to a single-arc feature after light soaking indeed is evidence of the reduction of resistance, leading to one less pair of resistor−capacitor in the fitting. We hypothesize that the reduction in resistance is due to the reduction of traps in the device after the light soaking process, which gives rise to better charge collection.

The shape transition of the Nyquist plot is also identified in ITIC-F-based device, as shown in Figure S5. This phenomenon is much less obvious in the ITIC-M device, indicating a much less trap distribution. This also explains why the light soaking effect is less significant in the ITIC-M device. Fitting parameters for the two detectors using the CPE component are summarized in Tables S3 and S4.

The light soaking is performed under white light from the tungsten lamp for the results discussed so far. It is critical to understand which wavelength is responsible for the light soaking effect. To deal with this problem, the photocurrent of the device (without soaking) under different wavelengths (370, 385, 600, 940, 1050, and 1550 nm) spanning from ultraviolet (UV) to shortwave infrared, is recorded to check the light soaking effect. Figure 3a shows the normalized photocurrent as a function of illumination time under different wavelengths. The light intensity for all of the wavelengths is controlled to be at similar levels to roll out the intensity dependency.

From the results, the photocurrent under UV light (e.g., 370 and 385 nm) is increasing as the illumination time gets longer. On the other hand, the photocurrent is independent of illumination time under visible and infrared light. This means that the UV photons from the broadband tungsten light are responsible for the light soaking effect in our devices.

It takes more than 100 s for the photocurrent to settle down under 385 nm. A shorter period of time is required for the photocurrent to stabilize under a shorter wavelength of 370 nm, at even lower light intensity. These results reveal that the light soaking effect is wavelength-dependent. It should be noted that there is a sharp increase in photocurrent upon 385 nm illumination, which is due to the fast response of the detector, followed by a slow increase owing to the light soaking effect. The instant photocurrent upon 370 nm illumination is low because of the less photoresponse at this wavelength.

It is also observed that this effect is intensity-dependent. Here, the intensity of the 370 nm light is tuned from 0.5 to 10.8 mW/cm^2, and the normalized photocurrent from a pristine device without light soaking is recorded and presented in Figure 3b. The photocurrent stabilizes faster under a higher intensity of UV light. It takes more than 200 s for the current to stabilize at a light intensity of 0.54 mW/cm^2, while only 6 s is required when the light intensity is up to 10.8 mW/cm^2. This is expected because there are more photons to eliminate the trap sites in the device.

From the results so far, it can be anticipated that the traps are deeply located within the bandgap of the semiconductors, which requires high-energy photons to mitigate. Meanwhile, it is interesting that the wavelengths of the UV photons used in the light soaking process are close to the transition state of the ZnO material.[47,48] It is observed in previous studies that the absorption and desorption processes of the oxygen molecules at the ZnO interface are possible, which is highly correlated to the conductivity of the ZnO layer.[47−49] Holes generated in the ZnO layer after absorption of UV photons would migrate to the locations where oxidizing molecules, e.g., oxygen, are absorbed by the ZnO layer, and neutralize the negatively charged oxidizing molecules, which can be regarded as a desorption process. This process would largely improve the surface conductivity of the ZnO layer. This process is highly possible in our devices, which contributes to the light soaking effect. But it should be noted that our devices are encapsulated after fabrication and the ZnO NP layer is covered with multiple layers instead of exposed directly to the air. It is thus anticipated that the absorption and desorption processes of the oxygen molecules are not as obvious as that in devices with active films directly exposed to the air.

The long-term effect of the light soaking process is also investigated. Here, the spectral response of the devices with and without light soaking is recorded as a function of aging time, as shown in Figure 3c. It is interesting that a 1 min exposition to the white light (∼20 mW/cm^2) from the tungsten lamp is enough to achieve the saturated photoresponse. However, for the time being, the photoresponse quickly shrinks to the pre-soaking level after 24 h. The light soaking effect is reversible[41] once the soaking time is not sufficient. By extending the light soaking time, e.g., 10 or 30 min, the degradation becomes less obvious. It should be noted that the light soaking effect is not permanent. The degradation of spectral responsivity from the device without light soaking is also compared to rule out the intrinsic degradation of the device. It is most probable that the degradation in the device after 10 or 30 min light soaking is from the sum of intrinsic degradation due to the imperfect encapsulation and the fading of the light soaking effect. It should be noted that prolonged light soaking may introduce traps in the organic device.[34,50]

The effect of light soaking on the transient response characteristics of the detector is also investigated. The transient photoresponse characteristics of the CDT-TQ:PC$_{71}$BM detector are plotted in Figure S6. The rise times are estimated to be 20.5 and 15 μs for the device without and with light soaking, corresponding to the 3 dB bandwidths of 23 and 40 kHz.

We also demonstrate the multifunctionality of the CDT-TQ:PC$_{71}$BM infrared detector as thermal sensor and photoplethysmography (PPG) sensor to show its potential for practical applications. The details can be found in the Supporting Information, and the results are presented in Figure S7.

CONCLUSIONS

This work studied the effects of light exposure, i.e., light soaking, on charge transport and collection in a narrow-bandgap organic photodetector. The analysis of the DOS distribution and impedance spectroscopy revealed deep trap reduction in the organic infrared detector after the light soaking process. As a result, the improvement in the photoresponse is observed, mainly due to the efficiency

https://doi.org/10.1021/acsphotonics.2c01504
ACS Photonics XXXX, XXX, XXX−XXX

enhancement in the photogenerated charge collection. It is also found that the light soaking effect is dependent on the light intensity and duration time of the soaking process. A few seconds of UV light soaking is viable to stabilize the photoresponse performances. The light soaking effect can be maintained for up to ∼24 h.

This work provides an analysis method to elucidate the effects of the light soaking process and quantify the changes in traps in the infrared detector, by illustrating trap distribution and quantity from experimental measurements and theoretical fittings. These results are inspiring and offer guidelines for device design and performance optimization in organic infrared detectors.

EXPERIMENTAL SECTION

J–V Fitting Model. The photocurrent (J_{ph}) in a photodiode can be described in the following equation[18]

$$J_{ph} = J_{sat} \cdot \eta_{diss} \cdot \eta_{coll}$$

where J_{ph} and J_{sat} are the photocurrent and saturation photocurrent at a specific light intensity, respectively, η_{diss} is the exciton dissociation efficiency, and η_{coll} is the charge collection efficiency.

The effective electric field is defined as $E_{eff} = (V_{built\text{-}in} - V_{app})/d$, where $V_{built\text{-}in}$ is the built-in voltage, V_{app} is the applied bias, and d is the thickness. The dissociation efficiency at an effective voltage can be described by the exciton dissociation rate (k_D) and recombination rate (k_R) in the form of

$$\eta_{diss}(E_{eff}) = \frac{k_D(E_{eff})}{k_D(E_{eff}) + k_R}$$

The exciton dissociation rate at effective electric field $k_D(E_{eff})$ is a function of binding energy (E_B), local carrier mobility (μ), electron/hole initial separation distance in an exciton (a = 1.2 nm), and the dielectric characteristics of the material, which can be expressed as follows

$$k_D(E_{eff}) = \frac{3q\mu}{4\pi\varepsilon_0\varepsilon_r a^3}\exp\left(-\frac{E_B}{kT}\right)\left(1 + b + \frac{b^2}{3} + \frac{b^3}{18} + \cdots\right)$$

where $E_B = \frac{q^2}{4\pi\varepsilon_0\varepsilon_r a}$, ε_0 and ε_r are the vacuum permittivity and dielectric constant (4.7) for the active layer, respectively, k is the Boltzmann constant, T is the temperature, and b is a parameter that is given in $b = \frac{q^3 E_{eff}}{8\pi\varepsilon_0\varepsilon_r k^2 T^2}$. Finally, the dissociation efficiency can be obtained by integrating $\eta_{diss}(E_{eff})$ over the electron–hole pair separation distance.[18]

From the Hecht model,[51] the charge collection efficiency is explained as

$$\eta_{coll} = \frac{2\mu\tau E_{eff}}{d}\left[1 - \exp\left(-\frac{d}{2\mu\tau E_{eff}}\right)\right]$$

where d represents the active layer thickness and $\mu\tau$ represents the mobility-lifetime product.

DOS Fitting Model. The density of states (DOS) distribution is obtained by analyzing the capacitance–frequency relationship.[17,34,36] The following equation describes the relation between DOS at energy E_ω and capacitance–frequency characteristics measured in a photodiode.

$$\mathrm{DOS}(E_\omega) = -\frac{V_{bi}}{qAtkT}\frac{\partial C(\omega)}{\partial \ln(\omega)}$$

In this equation, V_{bi} represents the built-in potential, q represents the elementary charge, A represents the active area, t represents the device thickness, k represents the Boltzmann constant, T represents the temperature, and $C(\omega)$ represents the capacitance of the diode at a particular angular frequency ω. The energy level for a trap state (E_ω) is defined as $E_\omega = kT\ln(\omega_0/\omega)$, where ω_0 represents the rate pre-factor for thermal excitation from the trap and is usually assumed to be 10^{12} s^{-1} in a typical organic photodiode.[34,52] It should be noted that this technique does not distinguish the trap type, either for holes or for electrons.

Impedance Spectroscopy. The constant phase element (CPE) is a mathematical component that accounts for the nonideality of the capacitor, and its impedance (Z_{CPE}) can be described as[53]

$$Z_{CPE} = \frac{1}{Q(j\cdot\omega)^n}$$

where $j = \sqrt{-1}$, ω is the radial frequency, and n and Q are constant numbers. When $0.7 < n < 1$, the CPE can be considered as an imperfect capacitor, and once $n = 1$, the CPE is reduced to the case of an ideal capacitor.[46,53]

ASSOCIATED CONTENT

Supporting Information

The Supporting Information is available free of charge at https://pubs.acs.org/doi/10.1021/acsphotonics.2c01504.

Experimental section; fitting parameters; energy diagrams; photoresponse, subgap states, and impedance for nonfullerene BHJ detectors; transient photoresponse, and bifunction demonstrations (PDF)

AUTHOR INFORMATION

Corresponding Authors

Ning Li − *School of Electronic and Optical Engineering, Nanjing University of Science and Technology, Nanjing 210094, China; Department of Electrical and Computer Engineering, University of California San Diego, La Jolla, California 92093-0407, United States;* orcid.org/0000-0003-3382-341X; Email: liningbox@outlook.com

Tse Nga Ng − *Department of Electrical and Computer Engineering, University of California San Diego, La Jolla, California 92093-0407, United States;* orcid.org/0000-0001-6967-559X; Email: tnn046@ucsd.edu

Authors

Naresh Eedugurala − *School of Polymer Science and Engineering, University of Southern Mississippi, Hattiesburg, Mississippi 39406, United States;* orcid.org/0000-0003-4714-7993

Jason D. Azoulay − *School of Polymer Science and Engineering, University of Southern Mississippi, Hattiesburg, Mississippi 39406, United States;* orcid.org/0000-0003-0138-5961

Complete contact information is available at: https://pubs.acs.org/10.1021/acsphotonics.2c01504

Author Contributions

N.L. and T.N.N. conceived the idea and designed the experiments. N.E. synthesized the CDT-TQ polymer under the supervision of J.D.A. N.L. carried out the fabrication and characterization of the devices. N.L. and T.N.N. wrote the manuscript. All of the authors contributed to the editing of the manuscript.

Funding

T.N.N. is grateful for the support from National Science Foundation award MCA-2120701. J.D.A. was supported by the Air Force Office of Scientific Research under the Organic Materials Chemistry Program (FA9550-17-1-0261) and by the National Science Foundation (OIA-1757220).

Notes

The authors declare no competing financial interest.

REFERENCES

(1) Bao, C.; Xu, W.; Yang, J.; Bai, S.; Teng, P.; Yang, Y.; Wang, J.; Zhao, N.; Zhang, W.; Huang, W.; Gao, F. Bidirectional Optical Signal Transmission between Two Identical Devices Using Perovskite Diodes. *Nat. Electron.* **2020**, *3*, 156−164.

(2) Tang, X.; Ackerman, M. M.; Chen, M.; Guyot-Sionnest, P. Dual-Band Infrared Imaging Using Stacked Colloidal Quantum Dot Photodiodes. *Nat. Photonics* **2019**, *13*, 277−282.

(3) Lin, Q.; Armin, A.; Burn, P. L.; Meredith, P. Filterless Narrowband Visible Photodetectors. *Nat. Photonics* **2015**, *9*, 687−694.

(4) Fuentes-Hernandez, C.; Chou, W. F.; Khan, T. M.; Diniz, L.; Lukens, J.; Larrain, F. A.; Rodriguez-Toro, V. A.; Kippelen, B. Large-Area Low-Noise Flexible Organic Photodiodes for Detecting Faint Visible Light. *Science* **2020**, *370*, 698−701.

(5) Li, N.; Mahalingavelar, P.; Vella, J. H.; Leem, D. S.; Azoulay, J. D.; Ng, T. N. Solution-Processable Infrared Photodetectors: Materials, Device Physics, and Applications. *Mater. Sci. Eng., R* **2021**, *146*, No. 100643.

(6) De Arquer, F. P.; Armin, A.; Meredith, P.; Sargent, E. H. Solution-Processed Semiconductors for next-Generation Photodetectors. *Nat. Rev. Mater.* **2017**, *2*, No. 16100.

(7) Yokota, T.; Zalar, P.; Kaltenbrunner, M.; Jinno, H.; Matsuhisa, N.; Kitanosako, H.; Tachibana, Y.; Yukita, W.; Koizumi, M.; Someya, T. Ultraflexible Organic Photonic Skin. *Sci. Adv.* **2016**, *2*, No. e1501856.

(8) Xu, Y.; Lin, Q. Photodetectors Based on Solution-Processable Semiconductors: Recent Advances and Perspectives. *Appl. Phys. Rev.* **2020**, *7*, No. 011315.

(9) Xing, S.; Kublitski, J.; Hänisch, C.; Winkler, L. C.; Li, T.-y.; Kleemann, H.; Benduhn, J.; Leo, K. Photomultiplication-Type Organic Photodetectors for Near-Infrared Sensing with High and Bias-Independent Specific Detectivity. *Adv. Sci.* **2022**, *9*, No. 2105113.

(10) Vella, J. H.; Huang, L.; Eedugurala, N.; Mayer, K. S.; Ng, T. N.; Azoulay, J. D. Broadband Infrared Photodetection Using a Narrow Bandgap Conjugated Polymer. *Sci. Adv.* **2021**, *7*, No. eabg2418.

(11) Yokota, T.; Nakamura, T.; Kato, H.; Mochizuki, M.; Tada, M.; Uchida, M.; Lee, S.; Koizumi, M.; Yukita, W.; Takimoto, A.; Someya, T. A Conformable Imager for Biometric Authentication and Vital Sign Measurement. *Nat. Electron.* **2020**, *3*, 113−121.

(12) Huang, J.; Lee, J.; Vollbrecht, J.; Brus, V. V.; Dixon, A. L.; Cao, D. X.; Zhu, Z.; Du, Z.; Wang, H.; Cho, K.; Bazan, G. C.; Nguyen, T. Q. A High-Performance Solution-Processed Organic Photodetector for Near-Infrared Sensing. *Adv. Mater.* **2020**, *32*, No. 1906027.

(13) Wu, Z.; Li, N.; Eedugurala, N.; Azoulay, J. D.; Leem, D. S.; Ng, T. N. Noise and Detectivity Limits in Organic Shortwave Infrared Photodiodes with Low Disorder. *npj Flexible Electron.* **2020**, *4*, No. 6.

(14) Lan, Z.; Lei, Y.; Chan, W. K. E.; Chen, S.; Luo, D.; Zhu, F. Near-Infrared and Visible Light Dual-Mode Organic Photodetectors. *Sci. Adv.* **2020**, *6*, No. eaaw8065.

(15) Lan, Z.; Zhu, F. Electrically Switchable Color-Selective Organic Photodetectors for Full-Color Imaging. *ACS Nano* **2021**, *15*, 13674−13682.

(16) Li, N.; Eedugurala, N.; Azoulay, J. D.; Ng, T. N. A Filterless Organic Photodetector Electrically Switchable between Visible and Infrared Detection. *Cell Rep. Phys. Sci.* **2022**, *3*, No. 100711.

(17) Wu, Z.; Zhai, Y.; Yao, W.; Eedugurala, N.; Zhang, S.; Huang, L.; Gu, X.; Azoulay, J. D.; Ng, T. N. The Role of Dielectric Screening in Organic Shortwave Infrared Photodiodes for Spectroscopic Image Sensing. *Adv. Funct. Mater.* **2018**, *28*, No. 1805738.

(18) Wu, Z.; Yao, W.; London, A. E.; Azoulay, J. D.; Ng, T. N. Elucidating the Detectivity Limits in Shortwave Infrared Organic Photodiodes. *Adv. Funct. Mater.* **2018**, *28*, No. 1800391.

(19) Tournebize, A.; Bussière, P. O.; Rivaton, A.; Gardette, J. L.; Medlej, H.; Hiorns, R. C.; Dagron-Lartigau, C.; Krebs, F. C.; Norrman, K. New Insights into the Mechanisms of Photodegradation/Stabilization of P3HT:PCBM Active Layers Using Poly(3-Hexyl- d 13-Thiophene). *Chem. Mater.* **2013**, *25*, 4522−4528.

(20) Mateker, W. R.; McGehee, M. D. Progress in Understanding Degradation Mechanisms and Improving Stability in Organic Photovoltaics. *Adv. Mater.* **2017**, *29*, No. 1603940.

(21) Classen, A.; Heumueller, T.; Wabra, I.; Gerner, J.; He, Y.; Einsiedler, L.; Li, N.; Matt, G. J.; Osvet, A.; Du, X.; Hirsch, A.; Brabec, C. J. Revealing Hidden UV Instabilities in Organic Solar Cells by Correlating Device and Material Stability. *Adv. Energy Mater.* **2019**, *9*, No. 1902124.

(22) Lee, H. K. H.; Telford, A. M.; Röhr, J. A.; Wyatt, M. F.; Rice, B.; Wu, J.; De Castro Maciel, A.; Tuladhar, S. M.; Speller, E.; McGettrick, J.; Searle, J. R.; Pont, S.; Watson, T.; Kirchartz, T.; Durrant, J. R.; Tsoi, W. C.; Nelson, J.; Li, Z. The Role of Fullerenes in the Environmental Stability of Polymer:Fullerene Solar Cells. *Energy Environ. Sci.* **2018**, *11*, 417−428.

(23) Kim, H. S.; Cook, J. B.; Lin, H.; Ko, J. S.; Tolbert, S. H.; Ozolins, V.; Dunn, B. Oxygen Vacancies Enhance Pseudocapacitive Charge Storage Properties of MoO3-X. *Nat. Mater.* **2017**, *16*, 454−462.

(24) Wöpke, C.; Göhler, C.; Saladina, M.; Du, X.; Nian, L.; Greve, C.; Zhu, C.; Yallum, K. M.; Hofstetter, Y. J.; Becker-Koch, D.; Li, N.; Heumüller, T.; Milekhin, I.; Zahn, D. R. T.; Brabec, C. J.; Banerji, N.; Vaynzof, Y.; Herzig, E. M.; MacKenzie, R. C. I.; Deibel, C. Traps and Transport Resistance Are the next Frontiers for Stable Non-Fullerene Acceptor Solar Cells. *Nat. Commun.* **2022**, *13*, No. 3786.

(25) Jiang, H.; Li, T.; Han, X.; Guo, X.; Jia, B.; Liu, K.; Cao, H.; Lin, Y.; Zhang, M.; Li, Y.; Zhan, X. Passivated Metal Oxide N-Type Contacts for Efficient and Stable Organic Solar Cells. *ACS Appl. Energy Mater.* **2020**, *3*, 1111−1118.

(26) Xu, X.; Li, D.; Yuan, J.; Zhou, Y.; Zou, Y. Recent Advances in Stability of Organic Solar Cells. *EnergyChem* **2021**, *3*, No. 100046.

(27) Burlingame, Q.; Huang, X.; Liu, X.; Jeong, C.; Coburn, C.; Forrest, S. R. Intrinsically Stable Organic Solar Cells under High-Intensity Illumination. *Nature* **2019**, *573*, 394−397.

(28) Duan, L.; Uddin, A. Progress in Stability of Organic Solar Cells. *Adv. Sci.* **2020**, *7*, No. 1903259.

(29) Liu, J.; Gao, M.; Kim, J.; Zhou, Z.; Chung, D. S.; Yin, H.; Ye, L. Challenges and Recent Advances in Photodiodes-Based Organic Photodetectors. *Mater. Today* **2021**, *51*, 475−503.

(30) Wang, Y.; Lan, W.; Li, N.; Lan, Z.; Li, Z.; Jia, J.; Zhu, F. Stability of Nonfullerene Organic Solar Cells: From Built-in Potential and Interfacial Passivation Perspectives. *Adv. Energy Mater.* **2019**, *9*, No. 1900157.

(31) Wang, Y.; Lee, J.; Hou, X.; Labanti, C.; Yan, J.; Mazzolini, E.; Parhar, A.; Nelson, J.; Kim, J. S.; Li, Z. Recent Progress and Challenges toward Highly Stable Nonfullerene Acceptor-Based Organic Solar Cells. *Adv. Energy Mater.* **2021**, *11*, No. 2003002.

(32) Jørgensen, M.; Norrman, K.; Gevorgyan, S. A.; Tromholt, T.; Andreasen, B.; Krebs, F. C. Stability of Polymer Solar Cells. *Adv. Mater.* **2012**, *24*, 580−612.

(33) Peters, C. H.; Sachs-Quintana, I. T.; Mateker, W. R.; Heumueller, T.; Rivnay, J.; Noriega, R.; Beiley, Z. M.; Hoke, E. T.;

https://doi.org/10.1021/acsphotonics.2c01504
ACS Photonics XXXX, XXX, XXX−XXX

Salleo, A.; McGehee, M. D. The Mechanism of Burn-in Loss in a High Efficiency Polymer Solar Cell. *Adv. Mater.* **2012**, *24*, 663−668.
(34) Street, R. A.; Yang, Y.; Thompson, B. C.; McCulloch, I. Capacitance Spectroscopy of Light Induced Trap States in Organic Solar Cells. *J. Phys. Chem. C* **2016**, *120*, 22169−22178.
(35) Simone, G.; Dyson, M. J.; Meskers, S. C. J.; Janssen, R. A. J.; Gelinck, G. H. Organic Photodetectors and Their Application in Large Area and Flexible Image Sensors: The Role of Dark Current. *Adv. Funct. Mater.* **2019**, *30*, No. 1904205.
(36) Kublitski, J.; Hofacker, A.; Boroujeni, B. K.; Benduhn, J.; Nikolis, V. C.; Kaiser, C.; Spoltore, D.; Kleemann, H.; Fischer, A.; Ellinger, F.; Vandewal, K.; Leo, K. Reverse Dark Current in Organic Photodetectors and the Major Role of Traps as Source of Noise. *Nat. Commun.* **2021**, *12*, No. 551.
(37) Abbaszadeh, D.; Kunz, A.; Kotadiya, N. B.; Mondal, A.; Andrienko, D.; Michels, J. J.; Wetzelaer, G. J. A. H.; Blom, P. W. M. Electron Trapping in Conjugated Polymers. *Chem. Mater.* **2019**, *31*, 6380−6386.
(38) Haneef, H. F.; Zeidell, A. M.; Jurchescu, O. D. Charge Carrier Traps in Organic Semiconductors: A Review on the Underlying Physics and Impact on Electronic Devices. *J. Mater. Chem. C* **2020**, *8*, 759−787.
(39) Small, C. E.; Chen, S.; Subbiah, J.; Amb, C. M.; Tsang, S. W.; Lai, T. H.; Reynolds, J. R.; So, F. High-Efficiency Inverted Dithienogermole-Thienopyrrolodione-Based Polymer Solar Cells. *Nat. Photonics* **2012**, *6*, 115−120.
(40) Xu, W.; Xia, R.; Ye, T.; Zhao, L.; Kan, Z.; Mei, Y.; Yan, C.; Zhang, X. W.; Lai, W. Y.; Keivanidis, P. E.; Huang, W. Understanding the Light Soaking Effects in Inverted Organic Solar Cells Functionalized with Conjugated Macroelectrolyte Electron-Collecting Interlayers. *Adv. Sci.* **2015**, *3*, No. 1500245.
(41) Lim, F. J.; Set, Y. T.; Krishnamoorthy, A.; Ouyang, J.; Luther, J.; Ho, G. W. Addressing the Light-Soaking Issue in Inverted Organic Solar Cells Using Chemical Bath Deposited Fluorinated TiOx Electron Transport Layer. *J. Mater. Chem. A* **2015**, *3*, 314−322.
(42) Nam, C. Y. Ambient Air Processing Causes Light Soaking Effects in Inverted Organic Solar Cells Employing Conjugated Polyelectrolyte Electron Transfer Layer. *J. Phys. Chem. C* **2014**, *118*, 27219−27225.
(43) Street, R. A. Electronic Structure and Properties of Organic Bulk-Heterojunction Interfaces. *Adv. Mater.* **2016**, *28*, 3814−3830.
(44) Shibayama, N.; Zhang, Y.; Satake, T.; Sugiyama, M. Modelling of an Equivalent Circuit for Cu2ZnSnS4- and Cu2ZnSnSe4-Based Thin Film Solar Cells. *RSC Adv.* **2017**, *7*, 25347−25352.
(45) Chung, C. C.; Narra, S.; Jokar, E.; Wu, H. P.; Wei-Guang Diau, E. Inverted Planar Solar Cells Based on Perovskite/Graphene Oxide Hybrid Composites. *J. Mater. Chem. A* **2017**, *5*, 13957−13965.
(46) McNealy, B. E.; Hertz, J. L. On the Use of the Constant Phase Element to Understand Variation in Grain Boundary Properties. *Solid State Ionics* **2014**, *256*, 52−60.
(47) Jin, Y.; Wang, J.; Sun, B.; Blakesley, J. C.; Greenham, N. C. Solution-Processed Ultraviolet Photodetectors Based on Colloidal ZnO Nanoparticles. *Nano Lett.* **2008**, *8*, 1649−1653.
(48) Jun, J. H.; Seong, H.; Cho, K.; Moon, B. M.; Kim, S. Ultraviolet Photodetectors Based on ZnO Nanoparticles. *Ceram. Int.* **2009**, *35*, 2797−2801.
(49) Verbakel, F.; Meskers, S. C. J.; Janssen, R. A. J. Surface Modification of Zinc Oxide Nanoparticles Influences the Electronic Memory Effects in ZnO-Polystyrene Diodes. *J. Phys. Chem. C* **2007**, *111*, 10150−10153.
(50) Patel, J. B.; Tiwana, P.; Seidler, N.; Morse, G. E.; Lozman, O. R.; Johnston, M. B.; Herz, L. M. Effect of Ultraviolet Radiation on Organic Photovoltaic Materials and Devices. *ACS Appl. Mater. Interfaces* **2019**, *11*, 21543−21551.
(51) Street, R. A.; Schoendorf, M.; Roy, A.; Lee, J. H. Interface State Recombination in Organic Solar Cells. *Phys. Rev. B* **2010**, *81*, No. 205307.
(52) Walter, T.; Herberholz, R.; Müller, C.; Schock, H. W. Determination of Defect Distributions from Admittance Measurements and Application to Cu(In,Ga)Se2 Based Heterojunctions. *J. Appl. Phys.* **1996**, *80*, 4411−4420.
(53) Wang, K.; Parekh, U.; Pailla, T.; Garudadri, H.; Gilja, V.; Ng, T. N. Stretchable Dry Electrodes with Concentric Ring Geometry for Enhancing Spatial Resolution in Electrophysiology. *Adv. Healthcare Mater.* **2017**, *6*, No. 1700552.

https://doi.org/10.1021/acsphotonics.2c01504
ACS Photonics XXXX, XXX, XXX−XXX